https://doi.org/10.5194/amt-2020-257
Preprint. Discussion started: 6 August 2020

Atmospheric Measurement Techniques Discussions

Quantifying fugitive gas emissions from an oil sands tailings pond with open-path FTIR measurements

Yuan You[1,§], Samar G. Moussa[1], Lucas Zhang[2], Long Fu[2], James Beck[3], Ralf M. Staebler[1]

[1] Air Quality Research Division, Environment and Climate Change Canada (ECCC), Toronto, M3H 5T4, Canada
[2]Alberta Environment and Parks, Edmonton, T5J, 5C6, Canada
[3]Suncor Energy Inc. , Calgary, T2P 3Y7, Canada
[§]Now at Department of Physics, University of Toronto, Toronto, M5S 1A7, Canada

Correspondence to: Ralf M. Staebler (ralf.staebler@canada.ca)

Abstract. Fugitive emissions from tailings ponds contribute significantly to facility emissions in the Alberta Oil Sands, but details on chemical emission profiles and the temporal and spatial variability of emissions to the atmosphere are sparse, since flux measurement techniques applied for compliance monitoring have their limitations. In this study, open-path Fourier transform infrared spectroscopy was evaluated as a potential alternative method for quantifying spatially representative fluxes for various pollutants (methane, ammonia, and alkanes) from a particular pond, using vertical flux gradient and inverse dispersion methods. Gradient fluxes of methane averaged 3.7 g $m^{-2}d^{-1}$ but were 40% lower than nearby eddy covariance measurements, while inverse dispersion fluxes agreed to within 11%. Significant NH_3 emission fluxes were observed (0.11 g $m^{-2}d^{-1}$ (92 tonnes y^{-1})), and total alkane fluxes were estimated to be 1.33 g $m^{-2}d^{-1}$ (1120 tonnes y^{-1}), representing 12% of the facility emissions.

1 Introduction

Tailings from the oil sands industrial processes in Alberta's Athabasca Oil Sands consist of a mixture of water, sand, non-recovered bitumen, and additives from the bitumen extraction processes (Small et al., 2015). These tailings are deposited into large engineered tailings ponds on site. Separation of processed water from remaining tailings occurs continuously in the tailings pond, and the processed water is recycled (Canada's Oil sands. Tailings Ponds: https://www.canadasoilsands.ca/en/explore-topics/tailings-ponds). The total liquid surface area covered by tailings ponds in the Athabasca Oil Sands was 103 km^2 in 2016 and continues to grow (Alberta Environment and Parks, 2016). Emissions to the atmosphere from tailings ponds include methane (CH_4), carbon dioxide (CO_2), reduced sulfur compounds, volatile organic compounds (VOCs), and polycyclic aromatic hydrocarbons (PAHs) (Siddique et al., 2007; Simpson et al., 2010; Yeh et al., 2010; Siddique et al., 2011; Siddique et al., 2012; Galarneau et al., 2014; Small et al., 2015; Bari and Kindzierski, 2018; Zhang et al., 2019). Emissions from tailings ponds vary with pond conditions, such as pond age and solvents additives in the ponds, and can contribute significantly to total facility emissions (Small et al., 2015).

Very few studies focusing on emissions of air pollutants from tailings ponds have been published (Galarneau et al., 2014; Small et al., 2015; Zhang et al., 2019). Compounds of particular interest include alkanes and ammonia (NH_3). Alkanes are part of the solvents used in the extraction process (Small et al., 2015), and can dominate VOCs emissions

https://doi.org/10.5194/amt-2020-257
Preprint. Discussion started: 6 August 2020

Atmospheric Measurement Techniques Discussions

from oil sands facilities (Li et al., 2017). Previously reported VOCs emissions by facilities had large uncertainties, especially from fugitive sources, due to limitations of the methods used to estimate emissions for compliance monitoring purposes (Li et al., 2017). VOCs in the atmosphere are important because of their effects on ambient ozone and secondary aerosol formation (Field et al., 2015; Kroll and Seinfeld, 2008). Emissions of NH_3 from tailings ponds to the atmosphere have not been published, although NH_3 has been observed in the oil sands region (Bytnerowicz, et al., 2012; Whaley et al., 2018). NH_3 emissions have important environmental implications, such as forming atmospheric aerosols with sulfuric acid (Kürten, et al., 2016) and affecting nitrogen deposition in the ecosystem (Makar, et al., 2018). This information is important for model simulations of critical loads of acidifying deposition in the ecosystem (Makar, et al., 2018). This field measurement project provided a great opportunity to continuously measure and to quantify tailings pond emissions over more than a month, especially for NH_3 and total alkanes.

Open-path Fourier transform infrared (OP-FTIR) spectroscopy has been considered a good candidate for an alternative method to monitor fugitive emissions from industrial or hazardous waste area sources, since the method is non-intrusive, integrates over long path-lengths, and has the ability to quantify several different gases of interest simultaneously and continuously (Marshall et al., 1994), without sample line issues . It has previously been used to quantify mole fractions of various air pollutants from different sources such as forest fires (Griffith et al., 1991; Yokelson et al., 1996; Yokelson et al., 1997; Goode et al., 1999; Yokelson, 1999; Yokelson et al., 2007; Burling et al., 2010; Johnson et al., 2010; Akagi et al., 2013; Yokelson et al., 2013; Akagi et al., 2014; Paton-Walsh et al., 2014; Smith et al., 2014), volcanoes (Horrocks et al., 1999; Oppenheimer and Kyle, 2008), industrial sites (Wu et al., 1995), harbours (Wiacek et al., 2018), and road vehicles (Bradley et al., 2000; Grutter et al., 2003; You et al., 2017). OP-FTIR measurements with vertically separated paths have previously been conducted to derive emission rate of air pollutants. Schäfer et al. (2012) deployed two OP-FTIR spectrometers with parallel paths 2.2 meter vertically apart at a grassland at Fuhrberg Germany, to measure nitrous oxide (N_2O) emissions with a flux-gradient method, and showed the calculated flux is comparable to the chamber measurements at the same grassland. Flesch et al. (2016) deployed OP-FTIR measurement with one spectrometer and two paths vertically separated by about 1 m on average ("slant path" configuration) at a cattle field in Alberta, Canada. They derived emission rates of N_2O and NH_3 by flux-gradient and inverse-dispersion methods, demonstrating the capability of OP-FTIR systems to measure emission rates of N_2O and NH_3. Following the flux-gradient method in Flesch et al. (2016), Bai et al. (2018) measured the flux of N_2O, NH_3, CH_4, and CO_2 from a vegetable farm in Australia by an OP-FTIR system with two paths vertically separated by 0.5 m on average. At the same vegetable farm, Bai et al. (2019) measured emission rates of N_2O by flux chambers and OP-FTIR "slant path" configuration with flux-gradient methods, and showed a large variation of the ratio of N_2O fluxes with these two measurements. Inverse dispersion models have also been applied to OP- FTIR measurements to quantify emission rates in previous studies (Flesch et al., 2004; Flesch et al., 2005; Bai et al., 2014; Hu et al., 2016; Shonkwiler and Ham, 2018).

Longer continuous coverage with a greater height difference between paths is one distinguishing feature of this study compared to previous research. The motivation of this work is to quantify emission rates of pollutants from one specific tailings pond by combining OP-FTIR measurements with micrometeorological methods. Emissions of CH_4, NH_3, and total alkanes as well as a comparison of gradient and inverse dispersion methods are presented in this study.

https://doi.org/10.5194/amt-2020-257
Preprint. Discussion started: 6 August 2020

Atmospheric Measurement Techniques Discussions

2 Open-path FTIR field measurements and methods for deriving fluxes

The main site of this study was on the south shore of Suncor Pond 2/3 (Fig. S1; 56°59'0.90"N, 111°30'30.30"W 305m ASL). Turbulent fluxes were measured on a mobile tower with sonic anemometers (model CSAT-3, Campbell Scientific, USA) at three levels at 8m, 18m, and 32m above ground. Vertical gradients of gaseous pollutant mole fractions were measured by drawing air from 4m, 8m, 18, 32m to instrumentation housed in a trailer on the ground. The sample inlet at 4m was on the roof of the main trailer beside the mobile tower. Amongst these instruments for gaseous pollutants, cavity ring-down spectroscopy (model G2311-f and model G2204, Picarro, USA) were included to measure the CH_4 eddy covariance flux and CH_4 mole fraction vertical profile and calibrate the mole fraction from OP-FTIR retrievals. A propeller anemometer (Model 05103-10, Campbell Scientific, USA) on the roof of the main trailer at 4m above ground provided an additional measurement of wind speed and direction. Measurements were conducted from July 28 to September 5, 2017. The FTIR spectrometer was located right beside the flux tower and the paths were along the south shore of the pond. This manuscript focuses on derived fluxes from the measurement of OP-FTIR. Other experimental details of the project can be found in You et al (2020).

2.1 Open-path Fourier transform infrared spectrometer (OP-FITR) system

The FTIR measurements were taken with a commercial Open Path FTIR Spectrometer (Open Path Air Monitoring System (OPS), Bruker, Germany), which was setup at 1.7m above the ground in a trailer. The infrared source is an air-cooled Globar. The emitted radiation is directed through the interferometer where it is modulated, travels along the measurement path (200m horizontal distance) to a retroreflector array that reflects the radiation, travels back to the spectrometer, and enters a Stirling-cooled mercury cadmium telluride (MCT) detector (monostatic configuration). Three retroreflectors were employed in this study: one near ground level (1m) on a tripod, and two at higher elevations on basket lifts, resulting in heights of reflectors of approximately 1m, 11m and 23m above ground. Three paths with these three retro-reflectors are referred as bottom, middle and top paths. The bottom retro-reflector was approximately twice the size of the upper two (59 vs. 30 reflector cubes). All retro-reflectors were cleaned with an alcohol solution once during the study, and the bottom mirror were rinsed with de-ionized water three times. Return signal strength decreased by around 65% during the 5-week study due to reflector deterioration, presumably mostly due to impaction by particulate matter. This reflector deterioration also decreased the signal-to-noise by around 67%, based on spectral retrievals for CH_4 , but did not affect the mean mole fractions measured.

In this study, spectra were measured at a resolution of 0.5 cm^{-1} with 250 scans co-added to increase signal-to-noise ratio, resulting in roughly a one-minute temporal resolution. Stray light spectra were recorded regularly by pointing the spectrometer away from the retroreflectors. This stray light spectrum accounts for radiation back to the detector from internal reflections inside the spectrometer, i.e. not from the retroreflector array, and was subtracted from all the measurement spectra before performing further analysis.

Spectral fitting was performed with OPUS_RS (Bruker), which uses a non-linear curve fitting algorithm (You et al., 2017). Spectral windows and interference gases for each gas (Table 1) were determined by optimizing capture of the absorption features while minimizing interferences. To further improve fittings, baselines were optimized through either linear or Gaussian fits under given spectral windows and interfering gases. For CH_4 and CO_2, temperature-

https://doi.org/10.5194/amt-2020-257
Preprint. Discussion started: 6 August 2020


Atmospheric Measurement Techniques Discussions

dependent reference files were used for fitting and retrieving mole fractions. For other pollutants, reference spectra at 296K were used and retrieved mole fractions were corrected for air density using measured ambient temperature and pressure. Retrieved CH_4 mole fractions from FTIR were then calibrated against CH_4 mole fractions from point cavity ring-down spectrometer (CRDS) measurements (Picarro G2204) at 4 m (Supplemental Material 2.1. Fig. S2). These calibrated CH_4 mole fractions from the FTIR were then used in flux calculations.

We also attempted to retrieve several other pollutants from measured FTIR spectra, but encountered insufficient signal-to-noise ratios, given the existing mole fractions at this location, variability in ambient H_2O vapor, etc. These pollutants include toluene, benzene, xylenes, sulfur dioxide, dimethyl sulfide, carbonyl sulfide, formic acid, and hydrogen cyanide. For these trace gases at this site, the detection limits of this open-path system were insufficient for flux calculations.

2.2 Method of deriving gradient flux

2.2.1 Gradient flux

Gradient flux estimates are derived from the vertical gradient of mole fractions and the associated turbulence, given by

$$F_c = -K_c \frac{\partial c}{\partial z} \quad (1)$$

where F_c is the gradient flux for a pollutant c, and $\frac{\partial c}{\partial z}$ is the vertical gradient of mole fractions. K_c is the eddy diffusivity, a transfer coefficient characterizing turbulent transport (Monin and Obukhov, 1954). In this study, the gradient flux of pollutants measured by the OP- FTIR system is calculated with the "modified Bowen Ratio" method (Meyers et al., 1996; Bolinius et al., 2016). Details on the calculation of eddy diffusivities and eddy covariance fluxes of CH_4, can be found in You et al. (2020).

In this study, vertical profiles of the CH_4 mole fractions varied over time and mostly showed linear vertical profiles when the wind was from the pond (Supplemental Material Section 2.2). In the following calculation, the vertical profiles of CH_4 and other gases are considered linear over the entire project. Therefore, the representative average height of the FTIR top path is taken as the height of the middle point (at 12 m). For a given period, K_c is dependent on the height above the surface (Monin and Obukhov, 1954). K_c for gradient flux calculated from the top and bottom FTIR paths has been adjusted linearly based on the $K_{c\_2,4}$ calculated from point measurements at 8m and 32m on the tower:

$$\frac{K_{c\_FTIR}}{K_{c\_2,4}} = \frac{\frac{1+12}{2}}{\frac{8+32}{2}} = 0.325 \quad (2)$$

The gradient flux is calculated by combining this K_{c_FTIR} with the mole fractions gradient between top and bottom path of FTIR in Eq (1). The difference between assuming linear and logarithmic vertical profiles of the mole fractions is

https://doi.org/10.5194/amt-2020-257
Preprint. Discussion started: 6 August 2020


Atmospheric Measurement Techniques Discussions

discussed in the Supplemental Material Section 2.2. The logarithmic vertical profile assumption resulted in fluxes that were on average 85% of the gradient flux calculated with linear vertical profiles.

In addition to calculating gradient fluxes by using CH_4 mole fractions gradient between top and bottom paths, gradient fluxes of CH_4 were also calculated by using mole fractions gradient between middle and bottom paths. Results show that gradient fluxes with top-bottom paths gradient and with middle-bottom paths gradients are consistent within 95% (Supplemental Material Section 2.2, Table S1). These results suggest the gradient fluxes in this study are not sensitive to which paths were chosen, and support the assumption of linear profiles.

2.2.2 Inverse dispersion fluxes

Inverse dispersion models (IDMs) can be used to derive emission rates estimates based on line-integrated or point mole fraction measurements downwind of a defined source. In this study, we used WindTrax 2.0 (Thunder Beach Scientific, http://www.thunderbeachscientific.com; Flesch et al., 1995; Flesch et al., 2004). Details on IDM calculations and resulting CH_4 fluxes were presented in You et al. (2020). IDM fluxes of NH_3 and total alkane are shown in this work for comparison with gradient fluxes. Meteorological inputs for calculating inverse dispersion fluxes of NH_3 and total alkane are the same as described in You et al. (2020) for CH_4 fluxes.

3 Results and discussion

3.1 Meteorological conditions

The measurement site including the OP-FTIR was at the south shore of the pond (Fig. S1), therefore the north wind (wind direction (WD) $\geq 286°$ or WD $\leq 76°$) was defined as the wind coming from the pond (You et al., 2020). The wind came from the north for about 22% of the entire measurement period (You et al. (2020) Fig. S1). There was no significant diurnal variation in wind direction during the study period (You et al. (2020) Fig. S2). Detailed ambient temperature, water surface temperature, wind speed, and other meteorological parameters can be found in You et al. (2020). As discussed in You et al. (2020), the warm pond surface resulted in continuing convective turbulence at night, resulting in continuing transport of pollutants from the pond into the atmosphere without significant diurnal variation. Gradient and IDM fluxes for NH_3 and total alkanes are averages for half hour periods when the wind came from the pond. The half-hour fluxes were binned into 16 wind direction sectors, and the area-weighted averages of fluxes from the pond were calculated as described in You et al. (2020).

3.2 Methane

Path-integrated mole fractions and associated gradient fluxes of CH_4 from OP-FTIR are presented here to test if the gradient fluxes derived from the mole fractions with OP-FTIR are comparable to CH_4 fluxes from eddy covariance and IDM methods (You et al. (2020)). The area-weighted flux statistics from different methods are summarized in Table 2. The path-integrated measurement from the FTIR bottom path clearly indicates that the CH_4 mole fraction was elevated when the wind was from the pond direction, while it was steady near 2 ppm when the wind was from

https://doi.org/10.5194/amt-2020-257
Preprint. Discussion started: 6 August 2020


Atmospheric Measurement Techniques Discussions

other directions (Fig. S3 and S4). In addition, a clear vertical gradient (Fig. S4), with mole fractions along the bottom path on the order of 0.5 ppm to 1ppm higher than mole fractions from the top path, identified the pond as the CH_4 source. The fact that the CH_4 mole fraction increased when the wind was from the pond direction, and decreased with height, clearly points to the pond as the dominant local source.

For comparison, vertical profiles of the CH_4 mole fraction by point measurements on the nearby tower are given in Supplemental Material Section 2.2. A linear vertical extrapolation of the profiles to the point where the mole fraction reaches 2.0 ppm (background levels) indicated a median plume height of 64m (Fig. S5 and Fig. S6).

The gradient flux derived from the OP-FTIR shows that the flux was minimal when the wind was from other directions, except for the sector centered at 270° (Fig. 1), which represented a mix of pond and shoreline influences). The average and interquartile ranges of fluxes in wind direction sectors centered at 315°, 337.5° and 0° are comparable. This gradient flux result is consistent with the eddy covariance fluxes measured on the adjacent flux tower (You et al. 2020), and these results also suggest that the pond is the main source of measured CH_4 fluxes. However, the sector centered at 292.5° shows average flux 76% and 65% greater than sectors centered at 315° and 337.5°. This is different from the EC fluxes which showed closer agreement between the 292.5°, 315°, 337.5° and 0° sectors (You et al., 2020, Fig. 7). The footprint of the eddy covariance fluxes measured on the adjacent flux tower at 18m was calculated by using the Flux Footprint Prediction (FFP) model in Kljun et al. (2015), and results showed the 80% contribution distance was typically within 1km which is closer to the main site than the north edge of pond liquid surface (Fig. S1; You et al. (2020)). The outfall was about 1.4 km from the main site. The discrepancy suggests that the footprint of the gradient method incorporated emissions from the outfall more clearly than the smaller footprint of the eddy covariance method.

FTIR CH_4 gradient fluxes and eddy covariance (EC) fluxes showed a linear correlation, but on average, the gradient fluxes were lower than the EC fluxes by 40% (r^2=0.56) (Fig. S8). In agreement with EC, the gradient flux showed no significant diurnal variations when the wind was from the pond (Fig. S9, with a relative standard deviation of 36%). To investigate the difference between CH_4 gradient fluxes derived from FTIR and EC fluxes, the latter were examined in relation to meteorological conditions, similar to the analysis presented in You et al. (2020). The analysis in You et al. (2020) showed no correlation between EC flux and friction velocity (u_*) or wind speed, while a weak correlation between gradient flux and wind speed is observed (You et al. (2020) Fig. S10). As described in Supplemental Material Section 2.2 (Fig. S5, S6, and S7), CH_4 vertical profiles were closer to linear when the wind speed was less than 6 m/s, and were more logarithmic with wind speed greater than 6 m/s. The sector centered at 292.5° was often associated with wind speeds greater than 6 m/s (21% of the time). The approximation of linear vertical profile could have overestimated the CH_4 flux with periods of high winds by 15%. This weak dependence of gradient flux on wind speed and elevated fluxes in sector 292.5° may be partially due to the observed dependence of CH_4 vertical profiles on wind speed.

Model calculations by Horst (1999) showed that the estimated footprint of a gradient flux measurement at the geometric mean height of the gradient is similar to the footprint of EC flux at that same height, for homogeneous upwind area sources. However, mole fraction footprints are significantly larger than perturbation (flux) footprints (Schmid, 1994), and some CH_4 sources on the far shore (e.g. the outfall) may have contributed to the upper path CH_4

https://doi.org/10.5194/amt-2020-257
Preprint. Discussion started: 6 August 2020


Atmospheric Measurement Techniques Discussions

mole fraction. This decreased the vertical gradient difference and thus the derived flux relative to the eddy covariance flux with its smaller footprint, since the latter is more likely to represent water surface emissions only. As an approximate estimation, the footprint of the path-integrated mole fraction of the top path is about 2.3 km (23m × 100, Flesch et al. (2016)), and this covers the whole pond including the north edge (Fig. S1).

Background mole fractions, upwind of the source under investigation, must be provided for the bLS calculations of CH_4 fluxes. We quantified these using two methods. First, the background mole fraction was determined with the FTIR measurements at the south of the pond, as follows: for most of the days, it was taken as the minimum CH_4 mole fraction from the FTIR bottom path on each day while the wind direction was between 180° and 240°. On Aug 7th and 30th, there was no half-hour period when the wind was from this sector, and the background mole fraction was chosen as the minimum mole fraction for the day. For Aug 1st, there was also no half-hour period for this sector, and the minimum of the day was 2.40 ppm, significantly greater than the minimum mole fraction of other days. Therefore, the background mole fraction of the previous day, 1.92 ppm was used for Aug 1st.

Alberta Environment and Parks (AEP) conducted OP- FTIR measurements (RAM2000 G2; KASSAY FSI, ITT Corp., Mohrsville, PA, USA) at the north side of the pond (Fig. S1), quantifying CH_4 to be used as the second estimate of background mole fractions. For most of the days, the half-hour averaged mole fractions were directly used as the background mole fractions. From Aug 3rd 22:00 to Aug 4th 13:30, Aug 6th 08:00 to 17:00, Aug 23rd 1:30 to 2:00, there were no data from AEP, so background mole fractions for these periods were picked as the interpolation of mole fractions before and after this period. In this approach, the bLS flux results can be negative when the AEP mole fraction is greater than the mole fraction from the measurements at the south shore, possibly due to influences by other emission sources in the surrounding area, gas diffusion under low wind speeds, plume inertia when wind directions changes suddenly, or instrument mismatch differences.

CH_4 IDM fluxes with background determined from the first approach (using measurements at the south of the pond) agreed with IDM fluxes with background determined from the second approach (using measurements at the north of the pond), with a linear regression r^2 of 0.92, and a slope of 0.90; there was a 20% difference between average fluxes from the two approaches (Fig. S11; Table S1). These results confirm that the CH_4 flux estimate from this inverse dispersion approach is consistent and that the first approach to determining backgrounds is appropriate. In the following results and discussion, IDM fluxes with background mole fractions from the first method are used.

IDM and EC flux showed good comparison (slope=0.93, r^2=0.46, You et al., (2020), Fig.8(b)). The interquartile range of the fluxes from these two methods overlap, and the mean IDM fluxes are 11% smaller than EC flux.

3.3 NH_3

The mole fraction of NH_3 was elevated when the wind was from the pond, but was mainly below 5 ppb when the wind was from the south (Fig. 2(a)). NH_3 gradient fluxes were significant when the wind came from the pond direction (Fig. 3(a)).

The time series of mole fraction vertical gradient of NH_3 and CH_4 were similar (Fig. S4). The NH_3 gradient flux and CH_4 gradient flux showed good correlation (r^2=0.8, Fig. 4). The diurnal variation in NH_3 gradient flux (relative standard deviation =74%) was stronger than for the CH_4 gradient flux (relative standard deviation =36%), with greater

https://doi.org/10.5194/amt-2020-257
Preprint. Discussion started: 6 August 2020


Atmospheric Measurement Techniques Discussions

fluxes from 13:00 to 18:00 MDT (Mountain Daylight savings Time) (Fig. S12 (a)). Previous studies showed tailings pond waters contained elevated NH_3 concentrations, which makes them potential sources of NH_3 to the atmosphere (Allen, 2008; Risacher et al., 2018). NH_3 in the pond is mainly produced through nitrate and/or nitrite reduction during microbial activities (Barton and Fauque, 2009; Collins et al., 2016). In addition, some of these nitrate and/or nitrite reduction microbes may also produce reduced sulfur (Barton and Fauque, 2009), and observed reduced sulfur and NH_3 from FTIR show good correlation (Moussa et al. 2020a). The water sample collected from Pond2/3 on August 2017 during this study was alkaline (pH = 8.0 ± 0.5), which also supports the emission of NH_3.

The average (median) flux in the sector centered at 292.5° was 61% (44%) and 73% (28%) more than the average (median) flux in the sectors centered at 315° and 337.5°. These suggest the high average flux in 281-304° is skewed by big spikes which are associated with the outfall (with wind directions in 281-304°), but the majority of NH_3 fluxes in the 281-304° wind sector correlated well with CH_4 fluxes which were less affected by the outfall. Although hydrotreating processes in upgraders remove most of the sulfur and nitrogen from the bitumen residue, a small amount of NH_3 might still be carried with the processed water and tailings (Bytnerowicz et al., 2010), and transported with the outfall liquid into the pond. The negative fluxes observed for the 67.5° sector may be due to elevated NH_3 plumes originating from the upgrader facility 3 km upwind in this direction, resulting in a negative gradient and thus deposition to the pond under some circumstances.

IDM fluxes of NH_3 were calculated the same way as CH_4, and show a weak correlation with CH_4 IDM fluxes (Fig. 4b). The NH_3 background mole fraction was based on the mean daily minimum, approximately 1ppb (Fig. 2). Vertical profiles of NH_3 mole fraction (Fig. S13) with northerly wind also show roughly linear profiles similar to CH_4. Profiles of sectors centered at 292.5° and 315° are linear. Therefore, the outfall on average did not significantly contribute to the NH_3 profile, i.e. the pond surface was the main source of NH_3. NH_3 fluxes from the gradient method were significantly less than from the IDM method. This difference is mostly due to the input background NH_3 mole fraction. The background NH_3 mole fraction was not measured, and could be greater than 1 ppb if there was any source to the north of the pond. Assuming the NH_3 gradient flux as a reference, different backgrounds were tested in IDM to match the mean gradient flux. A background of 7 ppb of NH_3 was required to close the gap between gradient and IDM fluxes. This seems large but cannot be verified, since there was no ground level measurement of NH_3 near the north of the pond. This illustrates the advantage of using either eddy covariance or gradient flux measurements, which are based on mole fraction fluctuations or gradients at a single location and are therefore independent of upwind background mole fraction.

3.4 Total alkane

Total alkane derived from FTIR spectra used butane and octane as two surrogates in this study, following the method in EPA OTM10 (Thoma et al., 2010). Results only reflect alkanes which have similar absorption features as butane and octane, and cannot accurately represent other VOCs. Total alkane fluxes from the pond were evident (Fig. 3(b)). A comparison to CH_4 fluxes showed only a weak correlation (r^2=0.3, Fig. S14), unlike the correlation between NH_3 and CH_4 (Fig. 4(a)). This difference can be explained by sources of alkane and CH_4 at this site. Figure 3(b) shows the average flux from the sector centered at 292.5° is 3.5 g m^{-2} d^{-1}, which is 2.43 and 3.33 times of the average fluxes

https://doi.org/10.5194/amt-2020-257
Preprint. Discussion started: 6 August 2020


Atmospheric Measurement Techniques Discussions

from the sectors centered at 315° and 337.5°. Figure 1 shows that the average fluxes from the sector centered at 292.5° is 1.76 and 1.64 times of the average fluxes from sectors centered at 315° and 337.5°. These results indicate that there was an enhanced contribution (26%) from around 281° to 304° to total alkane flux measured at the site, but not to the observed CH_4 flux. This enhancement of alkane flux is likely due to the outfall, which was at the edge of the pond, 1.9 km from the site at 295°. The liquid mixture flowing into the pond contained naphthenic solvent which include a mixture of alkanes, alkenes, and aromatic hydrocarbons, and since the outfall is at a temperature of approximately 33° C, enhanced evaporation of volatile components can be expected from this area. The outfall also introduces some mechanical mixing in the upper layers of the pond water, which may contribute to elevated emission rates. The diurnal variation of total alkane gradient flux when the wind came from the pond direction was also weak (the standard deviation of average fluxes at each hour is comparable to the interquartile ranges, Fig. S15). The vertical profiles of total alkane mole fraction with northeastern winds were vertically invariant (Fig. S16). With northwestern winds, profiles showed a decrease mole fraction from bottom to middle path and minimal decrease or even increase from middle to the top path. These total alkane vertical profiles with northern wind, which are different from CH_4 or NH_3 profiles, suggesting there were additional sources other than the pond surface to measured total alkane flux, such as the outfall, and industrial activities upwind.

3.5 Methanol CH_3OH

Unlike pollutants studied above, the CH_3OH mole fraction did not show significant enhancement when wind was from the pond (Fig. S17), suggesting the pond was not significantly contributing to CH_3OH compared to potential sources surrounding the pond. The lifetime of CH_3OH is around 10 days (Simpson et al., 2011; Shephard et al., 2015), and the main source is vegetation (Millet et al., 2008). The mole fractions observed at the site were consistent with satellite measurements representative of the general oil sand region (Shephard et al., 2015), and with an airborne study of VOCs (Simpson et al., 2010). In addition to emissions from vegetation, CH_3OH observed in the oil sands region could be due to transport from biomass burning (Simpson et al., 2011; Bari and Kindzierski, 2018), and local traffic (Rogers et al., 2006; You et al., 2017).

3.6 Comparison of calculated fluxes to reported emissions and approaches

As a test of the robustness of these results, fluxes of CH_4, NH_3 and total alkane are also calculated from the "slant path" method described by Flesch et al. (2016). Calculation inputs and results are summarized in the Supplemental Material Section 6. Compared to gradient flux results with our modified Bowen ratio approach, CH_4, NH_3, and total alkane fluxes with the "slant path" flux-gradient method were 27%, 40%, and 56% smaller (Table S1). The difference in fluxes from the two approaches could be due to differences in assumptions regarding the vertical profiles. In our modified Bowen ratio gradient flux approach, we used linear vertical mole fraction profiles of pollutants to calculate the difference of mean heights between the two paths. In Flesch et al. (2016) the gradient flux for pairs of points along the two paths was integrated along the entire path length assuming the flux was uniform horizontally. In that approach, the dependence of K_c on height is incorporated explicitly, assuming a logarithmic wind profile including a stability

https://doi.org/10.5194/amt-2020-257
Preprint. Discussion started: 6 August 2020


Atmospheric Measurement Techniques Discussions

correction. In our modified Bowen ratio approach, K_c is derived from a measured and stability corrected K_m, and therefore did not require a wind profile shape assumption.

To facilitate a transparent comparison of the emission results from this study to reported facility wide emissions of Suncor, we present emission rates based on simple extrapolation of the measured August emissions to the whole year. Other possible seasonal emission profiles have been reported (Small et al., 2015); using these to convert from August emissions to annual average values would for example result in a scale factor of 0.92 (mass transfer model), 0.64 (mass transfer model adjusted for ice cover), or 0.42 (thawing degree-day model) (Cumulative Environmental Management Association, 2011). The seasonally invariant total emission estimate for NH_3 and total alkanes from Pond 2/3 to the air were 92 and 1120 tonnes y^{-1} in 2017. However, NH_3 emissions from Pond 2/3 have not been reported in the past, because NH_3 was not being measured as part of compliance flux chamber monitoring. Therefore, the facility wide NH_3 emissions reported to the Government of Canada National Pollutant Release Inventory (NPRI) (0.82 tonnes y^{-1}) in 2017 did not include fugitive emissions from tailings ponds. The solvents entering this tailings pond are naphtha additives with octane, nonane and heptane as the biggest contributors. Li et al. (2017) quantified alkane emissions (including n-alkanes, branched-alkanes, and cycloalkanes) as 36.2 tonne d^{-1} from the whole facility using airborne measurements in 2013, which is 73.9% of 49 tonne d^{-1} total VOC emission. Based on the VOC profile shown in Moussa et al. (2020b), heptane and octane were the highest emitted VOCs, and alkanes account for 54% of total VOC emitted from Pond2/3 in 2017. If we use reported facility wide VOC annual emissions in 2017 (17242 tonnes y^{-1}, NPRI) to estimate facility wide total alkane annual emission, we obtain 17242 × 53% = 9138 tonnes y^{-1}, and total alkane emissions from Pond2/3 contribute 12.2% to facility wide emissions for 2017. The fugitive NH_3 emissions from Pond2/3 in this study were 92 tonnes y^{-1}, a number that is 113 times the process related emission number reported for the facility to NPRI. Negligible volume of ammonia may be carried over to the pond through the naphtha recovery unit and FTT line and it is believed that the ammonia is mainly generated from the biogenic activities in the MFT layer of the pond. The majority of H_2S, NH_3 and CH_4 emissions are related to microbiological activities as evidenced in this study.

4 Conclusions and Implications

We have shown that OP-FTIR is an effective method to quantify mole fractions and vertical gradients of CH_4, NH_3, and total alkanes continuously and simultaneously for an area source such as a tailings pond. Benefits are the integration of mole fractions over long path lengths, thus providing a spatially representative average, and the avoidance of sample line issues that can be serious problems for sticky gases such as NH_3. Results from gradient (modified Bowen ratio) method and IDM calculations suggest OP-FTIR is a useful tool for deriving emission rates of CH_4, NH_3 and total alkane from this type of fugitive area source. For the two approaches of determining background mole fractions of CH_4 with the IDM method, i.e., upwind background measurement vs. local background estimation, the area weight-averaged fluxes of CH_4 were within 20%. FTIR CH_4 gradient fluxes and EC fluxes showed a linear correlation, but on average, the gradient fluxes were lower than the EC fluxes by 40%. IDM and EC flux showed good comparison, and the mean IDM fluxes are 11% smaller than EC flux. NH_3 gradient flux and IDM flux showed a difference of more than 50%, which suggests that there may have been sources of NH_3 upwind (north) of the pond

https://doi.org/10.5194/amt-2020-257
Preprint. Discussion started: 6 August 2020

Atmospheric Measurement Techniques Discussions

that were not captured by assuming that southern and northern background NH_3 were similar, thus illustrating a limitation of the IDM method. CH_4, NH_3, and total alkane fluxes were also calculated using the "slant path" flux-gradient method (Flesch et al. 2016), to compare to the modified Bowen ratio approach, and results were 27%, 40%, and 56% lower than the modified Bowen ratio approach.

The NH_3 emissions results in this study are the first to quantify NH_3 fugitive fluxes from a tailings pond and clearly showed that Pond2/3 is a significant source of NH_3, most likely through microbial activities in the pond. This suggests that at least some tailings ponds in the oil sands could be significant sources of NH_3, compared to process-related facility emissions. Further measurements of NH_3 emissions from tailings ponds are recommended to elucidate our understanding of the mechanisms behind NH_3 emissions and to improve the total facility emission estimates reported to NPRI.

Total alkane gradient fluxes from OP-FTIR measurements clearly showed that the pond is a significant source of total alkane. Annual alkane emissions extrapolated from these measurements represented 12.2% of facility emissions. The outfall area contributed significantly (26%) to pond alkane emissions, showing spatial variability of alkane emissions from the pond. Observed CH_3OH mole fractions show that the pond was unlikely a significant source of CH_3OH. This study demonstrated the applicability of OP-FTIR combined with modified Bowen ratio or inverse dispersion methods for determining emission fluxes of multiple gases simultaneously, with high temporal resolution and comprehensive spatial coverage.

Data availability.

All data are publicly available at http://data.ec.gc.ca/data/air/monitor/source-emissions-monitoring-oil-sands-region/emissions-from-tailings-ponds-to-the-atmosphere-oil-sands-region/.

Author contributions.

YY and RS wrote the manuscript; SM, LZ, LF and JB contributed data and comments.

Competing interests.

Dr. Beck is an employee of Suncor Energy. The other authors have no competing interests.

Acknowledgements.

The authors thank the technical team of Andrew Sheppard, Roman Tiuliugenev, Raymon Atienza and Raj Santhaneswaran for their invaluable contributions throughout, Julie Narayan for spatial analysis, Stewart Cober for management and Stoyka Netcheva for home base logistical support. We thank Suncor and its project team (Dan Burt et al.), AECOM (April Kliachik, Peter Tkalec) and SGS (Nathan Grey, Ardan Ross) for site logistics support. This work was partially funded under the Oil Sands Monitoring Program and is a contribution to the program but does not necessarily reflect the position of the program. We also acknowledge funding from the Program for Energy Research and Development (Natural Resources Canada) and from the Climate Change and Air Pollution Program (ECCC).

References

Alberta Environment and Parks, Total Area of the Oil Sands Tailings Ponds over Time: http://osip.alberta.ca/library/Dataset/Details/542, 2016. Last accessed: Sept 22, 2019.

Canada's Oil sands. Tailings Ponds: https://www.canadasoilsands.ca/en/explore-topics/tailings-ponds, Last accessed: Sept 29th, 2019.

Akagi, S. K., Yokelson, R. J., Burling, I. R., Meinardi, S., Simpson, I., Blake, D. R., McMeeking, G. R., Sullivan, A., Lee, T., Kreidenweis, S., Urbanski, S., Reardon, J., Griffith, D. W. T., Johnson, T. J., and Weise, D. R.: Measurements of reactive trace gases and variable O_3 formation rates in some South Carolina biomass burning plumes, Atmos. Chem. Phys., 13, 1141-1165, http://doi.org/10.5194/acp-13-1141-2013, 2013.

Akagi, S. K., Burling, I. R., Mendoza, A., Johnson, T. J., Cameron, M., Griffith, D. W. T., Paton-Walsh, C., Weise, D. R., Reardon, J., and Yokelson, R. J.: Field measurements of trace gases emitted by prescribed fires in southeastern US pine forests using an open-path FTIR system, Atmos. Chem. Phys., 14, 199-215, http://doi.org/10.5194/acp-14-199-2014, 2014.

Allen, E. W.: Process water treatment in Canada's oil sands industry: I. Target pollutants and treatment objectives, J. Environ. Eng. Sci., 7, 123-138, http://doi.org/10.1139/S07-038, 2008.

Bai, M., Suter, H., Lam, S. K., Sun, J., and Chen, D.: Use of open-path FTIR and inverse dispersion technique to quantify gaseous nitrogen loss from an intensive vegetable production site, Atmos. Environ., 94, 687-691, http://doi.org/10.1016/j.atmosenv.2014.06.013, 2014.

Bai, M., Suter, H., Lam, S. K., Davies, R., Flesch, T. K., and Chen, D.: Gaseous emissions from an intensive vegetable farm measured with slant-path FTIR technique, Agric. For. Meterol., 258, 50-55, http://doi.org/10.1016/j.agrformet.2018.03.001, 2018.

Bai, M., Suter, H., Lam, S. K., Flesch, T. K., and Chen, D.: Comparison of slant open-path flux gradient and static closed chamber techniques to measure soil N_2O emissions, Atmos. Meas. Tech., 12, 1095-1102, http://doi.org/10.5194/amt-12-1095-2019, 2019.

Bari, M. A., and Kindzierski, W. B.: Ambient volatile organic compounds (VOCs) in communities of the Athabasca oil sands region: Sources and screening health risk assessment, Environ. Pollut., 235, 602-614, http://doi.org/10.1016/j.envpol.2017.12.065, 2018.

Bolinius, D. J., Jahnke, A., and MacLeod, M.: Comparison of eddy covariance and modified Bowen ratio methods for measuring gas fluxes and implications for measuring fluxes of persistent organic pollutants, Atmos. Chem. Phys., 16, 5315-5322, http://doi.org/10.5194/acp-16-5315-2016, 2016.

Bradley, K. S., Brooks, K. B., Hubbard, L. K., Popp, P. J., and Stedman, D. H.: Motor vehicle fleet emissions by OP-FTIR, Environ. Sci. Tech., 34, 897-899, http://doi.org/10.1021/es9909226, 2000.

Burling, I. R., Yokelson, R. J., Griffith, D. W. T., Johnson, T. J., Veres, P., Roberts, J. M., Warneke, C., Urbanski, S. P., Reardon, J., Weise, D. R., Hao, W. M., and De Gouw, J.: Laboratory measurements of trace gas emissions

https://doi.org/10.5194/amt-2020-257
Preprint. Discussion started: 6 August 2020

from biomass burning of fuel types from the southeastern and southwestern United States, Atmos. Chem. Phys., 10, 11115-11130, http://doi.org/10.5194/acp-10-11115-2010, 2010.

Bytnerowicz, A., Fraczek, W., Schilling, S., and Alexander, D.: Spatial and temporal distribution of ambient nitric acid and ammonia in the Athabasca Oil Sands Region, Alberta, J. Limnol., 69, 11-21, 10.3274/JL10-69-S1-03, 2010.

Collins, C. E. V., Foght, J. M., and Siddique, T.: Co-occurrence of methanogenesis and N_2 fixation in oil sands tailings, Sci. Total Environ., 565, 306-312, https://doi.org/10.1016/j.scitotenv.2016.04.154, 2016.

Cumulative Environmental Management Association: Protocol for Updating and Preparing a Modelling Emission Inventory, http://library.cemaonline.ca/ckan/dataset/4cbfe171-aab8-49f8-8d67-118e6840d974/resource/8f449c5d-3129-4d6f-a530-46ec33a46208/download/protocolforupdatingandpreparingamodelling.pdf, 2011. Last accessed Feb 26, 2020.

Field, R.A., Soltis, J., McCarthy, M. C., Murphy, S., and Montague, D. C.: Influence of oil and gas field operations on spatial and temporal distributions of atmospheric non-methane hydrocarbons and their effects on ozone formation in winter, Atmos. Chem. Phys., 15, 3527-3542, https://doi.org/10.5194/acp-15-3527-2015, 2015.

Flesch, T., Wilson, J., Harper, L., and Crenna, B.: Estimating gas emissions from a farm with an inverse-dispersion technique, Atmos. Environ., 39, 4863-4874, http://doi.org/10.1016/j.atmosenv.2005.04.032, 2005.

Flesch, T. K., Wilson, J. D., and Yee, E.: Backward-time Lagrangian stochastic dispersion models and their application to estimate gaseous emissions, J. Appl. Meteorol., 34, 1320-1332, https://doi.org/10.1175/1520-0450(1995)034<1320:BTLSDM>2.0.CO;2, 1995.

Flesch, T. K., Wilson, J. D., Harper, L. A., Crenna, B. P., and Sharpe, R. R.: Deducing ground-to-air emissions from observed trace gas concentrations: A field trial, J. Appl. Meteorol., 43, 487-502, https://doi.org/10.1175/1520-0450(2004)043<0487:DGEFOT>2.0.CO;2, 2004.

Flesch, T. K., Baron, V. S., Wilson, J. D., Griffith, D. W. T., Basarab, J. A., and Carlson, P. J.: Agricultural gas emissions during the spring thaw: Applying a new measurement technique, Agric. For. Meterol., 221, 111-121, https://doi.org/10.1016/j.agrformet.2016.02.010, 2016.

Foght, J. M., Gieg, L. M., and Siddique, T.: The microbiology of oil sands tailings: Past, present, future, FEMS Microbiol. Ecol., 93, https://doi.org/10.1093/femsec/fix034, 2017.

Galarneau, E., Hollebone, B. P., Yang, Z., and Schuster, J.: Preliminary measurement-based estimates of PAH emissions from oil sands tailings ponds, Atmos. Environ., 97, 332-335, https://doi.org/10.1016/j.atmosenv.2014.08.038, 2014.

Goode, J. G., Yokelson, R. J., Susott, R. A., and Ward, D. E.: Trace gas emissions from laboratory biomass fires measured by open-path Fourier transform infrared spectroscopy: Fires in grass and surface fuels, J. Geophys. Res., 104, 21237-21245, https://doi.org/10.1029/1999JD900360, 1999.

Government of Canada, National Pollutant Release Inventory: https://pollution-waste.canada.ca/national-release-inventory/archives/index.cfm?do=facility_substance_summary&lang=en&opt_npri_id=0000002230&opt_report_year=2017. Last access: Jan 07, 2020.

https://doi.org/10.5194/amt-2020-257
Preprint. Discussion started: 6 August 2020

Griffith, D. W. T., Mankin, W. G., Coffey, M. T., Ward, D. E., and RieBau, A.: "FTIR remote sensing of biomass burning emissions of CO_2, CO, CH_4, CH_2O, NO, NO_2, NH_3, and N_2O." Global biomass burning: atmospheric, alimate, and biospheric implications., MIT Press., Cambridge, MA, 1991.

Grutter, M., Flores, E., Basaldud, R., and Ruiz-Suarez, L. G.: Open-path FTIR spectroscopic studies of the trace gases over Mexico City, Atmos. Oceanic Opt., 16, 232-236, 2003.

Horrocks, L., Burton, M., Francis, P., and Oppenheimer, C.: Stable gas plume composition measured by OP-FTIR spectroscopy at Masaya Volcano, Nicaragua, 1998-1999, Geophys. Res. Lett,, 26, 3497-3500, https://doi.org/10.1029/1999GL008383, 1999.

Horst, T. W.: The footprint for estimation of atmosphere-surface exchange fluxes by profile techniques, Boundary Layer Meteorol., 90, 171-188, https://doi.org/10.1023/A:1001774726067, 1999.

Hu, N., Flesch, T. K., Wilson, J. D., Baron, V. S., and Basarab, J. A.: Refining an inverse dispersion method to quantify gas sources on rolling terrain, Agric. For. Meterol., 225, 1-7, https://doi.org/10.1016/j.agrformet.2016.05.007, 2016.

Johnson, T. J., Profeta, L. T. M., Sams, R. L., Griffith, D. W. T., and Yokelson, R. L.: An infrared spectral database for detection of gases emitted by biomass burning, Vib. Spectrosc., 53, 97-102, https://doi.org/10.1016/j.vibspec.2010.02.010, 2010.

Kljun, N., Calanca, P., Rotach, M. W., and Schmid, H. P.: A simple two-dimensional parameterisation for Flux Footprint Prediction (FFP), Geosci. Model Dev., 8, 3695-3713, https://doi.org/10.5194/gmd-8-3695-2015, 2015.

Kroll, J, and Seinfeld, J. H.: Chemistry of secondary organic aerosol: Formation and evolution of low-volatility organics in the atmosphere, Atmos. Environ., 3593-3624, https://doi.org/10.1016/j.atmosenv.2008.01.003, 2008.

Kürten, A., Bianchi, F., Almeida, J., Kupiainen-Määttä, O., Dunne, E. M., Duplissy, J., Williamson, C., Barmet, P., Breitenlechner, M., Dommen, J., Donahue, N. M., Flagan, R. C., Franchin, A., Gordon, H., Hakala, J., Hansel, A., Heinritzi, M., Ickes, L., Jokinen, T., Kangasluoma, J., Kim, J., Kirkby, J., Kupc, A., Lehtipalo, K., Leiminger, M., Makhmutov, V., Onnela, A., Ortega, I. K., Petäjä, T., Praplan, A. P., Riccobono, F., Rissanen, M. P., Rondo, L., Schnitzhofer, R., Schobesberger, S., Smith, J. N., Steiner, G., Stozhkov, Y., Tomé, A., Tröstl, J., Tsagkogeorgas, G., Wagner, P. E., Wimmer, D., Ye, P., Baltensperger, U., Carslaw, K., Kulmala, M., and Curtius, J.: Experimental particle formation rates spanning tropospheric sulfuric acid and ammonia abundances, ion production rates, and temperatures, J. Geophys. Res., 121, 12,377-312,400, https://doi.org/10.1002/2015JD023908, 2016.

Li, S. M., Leithead, A., Moussa, S. G., Liggio, J., Moran, M. D., Wang, D., Hayden, K., Darlington, A., Gordon, M., Staebler, R., Makar, P. A., Stroud, C. A., McLaren, R., Liu, P. S. K., O'Brien, J., Mittermeier, R. L., Zhang, J., Marson, G., Cober, S. G., Wolde, M., and Wentzell, J. J. B.: Differences between measured and reported volatile organic compound emissions from oil sands facilities in Alberta, Canada, Proc. Natl. Acad. Sci. U. S. A., 114, E3756-E3765, https://doi.org/10.1073/pnas.1617862114, 2017.

Liggio, J., Moussa, S. G., Wentzell, J., Darlington, A., Liu, P., Leithead, A., Hayden, K., O'Brien, J., Mittermeier, R. L., Staebler, R., Wolde, M., and Li, S. M.: Understanding the primary emissions and secondary formation of gaseous organic acids in the oil sands region of Alberta, Canada, Atmos. Chem. Phys., 17, 8411-8427, https://doi.org/10.5194/acp-17-8411-2017, 2017.

https://doi.org/10.5194/amt-2020-257
Preprint. Discussion started: 6 August 2020

Makar, P. A., Akingunola, A., Aherne, J., Cole, A. S., Aklilu, Y. A., Zhang, J., Wong, I., Hayden, K., Li, S. M., Kirk, J., Scott, K., Moran, M. D., Robichaud, A., Cathcart, H., Baratzedah, P., Pabla, B., Cheung, P., Zheng, Q., and Jeffries, D. S.: Estimates of exceedances of critical loads for acidifying deposition in Alberta and Saskatchewan, Atmos. Chem. Phys., 18, 9897-9927, https://doi.org/10.5194/acp-18-9897-2018, 2018.

Marshall, T. L., Chaffin, C. T., Hammaker, R. M., and Fateley, W. G.: An introduction to open-path FT-IR atmospheric monitoring, Environ. Sci. Technol., 28, 5, 224-232, https://doi.org/10.1021/es00054a715, 1994.

Meyers, T. P., Hall, M. E., Lindberg, S. E., and Kim, K.: Use of the modified bowen-ratio technique to measure fluxes of trace gases, Atmos. Environ., 30, 3321-3329, https://doi.org/10.1016/1352-2310(96)00082-9, 1996.

Millet, D. B., Jacob, D. J., Custer, T. G., De Gouw, J. A., Goldstein, A. H., Karl, T., Singh, H. B., Sive, B. C., Talbot, R. W., Warneke, C., and Williams, J.: New constraints on terrestrial and oceanic sources of atmospheric methanol, Atmos. Chem. Phys., 8, 6887-6905, https://doi.org/10.5194/acp-8-6887-2008, 2008.

Monin, A. S., and Obukhov, A. M.: Basic laws of turbulent mixing in the surface layer of the atmosphere, Contrib. Geophys. Inst. Acad. Sci. USSR, 24, 25, 1954.

Moussa, S.G., Staebler, R.M. You, Y., Leithead, A., Mittermeier, R., Hayden, K., Mihele, C., and Beck, J.: Total Reduced Sulfur Fugitive Emissions from an Oil Sands Tailings Pond: Sources and Estimates. In preparation, Atmos. Env., 2020a.

Moussa, S.G., Staebler, R.M., You, Y., Leithead, A., Yousif, M.A., Brickell, P., Beck, J. Jiang, Z., Li, S.-M., Liggio, J., Wren, S.N., Darlington, A., and Narayan, J.: Fugitive Emissions of Volatile Organic Compounds from a Tailings Pond in the Oil Sands Region of Alberta. In preparation, Env. Sci. Tech., 2020b.

Oppenheimer, C., and Kyle, P. R.: Probing the magma plumbing of Erebus volcano, Antarctica, by open-path FTIR spectroscopy of gas emissions, J. Volcanol. Geotherm. Res., 177, 743-754, https://doi.org/10.1016/j.jvolgeores.2007.08.022, 2008.

Paton-Walsh, C., Smith, T. E. L., Young, E. L., Griffith, D. W. T., and Guérette, É. A.: New emission factors for Australian vegetation fires measured using open-path Fourier transform infrared spectroscopy - Part 1: Methods and Australian temperate forest fires, Atmos. Chem. Phys., 14, 11313-11333, https://doi.org/10.5194/acp-14-11313-2014, 2014.

Penner, T. J., and Foght, J. M.: Mature fine tailings from oil sands processing harbour diverse methanogenic communities, Can. J. Microbiol., 56, 459-470, https://doi.org/10.1139/W10-029, 2010.

Risacher, F. F., Morris, P. K., Arriaga, D., Goad, C., Nelson, T. C., Slater, G. F., and Warren, L. A.: The interplay of methane and ammonia as key oxygen consuming constituents in early stage development of Base Mine Lake, the first demonstration oil sands pit lake, Appl. Geochem., 93, 49-59, https://doi.org/10.1016/j.apgeochem.2018.03.013, 2018.

Rogers, T. M., Grimsrud, E. P., Herndon, S. C., Jayne, J. T., Kolb, C. E., Allwine, E., Westberg, H., Lamb, B. K., Zavala, M., Molina, L. T., Molina, M. J., and Knighton, W. B.: On-road measurements of volatile organic compounds in the Mexico City metropolitan area using proton transfer reaction mass spectrometry, Int. J. Mass Soectrom., 252, 26-37, https://doi.org/10.1016/j.ijms.2006.01.027, 2006.

https://doi.org/10.5194/amt-2020-257
Preprint. Discussion started: 6 August 2020

Schäfer, K., Grant, R. H., Emeis, S., Raabe, A., von der Heide, C., and Schmid, H. P.: Areal-averaged trace gas emission rates from long-range open-path measurements in stable boundary layer conditions, Atmos. Meas. Tech., 5, 1571-1583, https://doi.org/10.5194/amt-5-1571-2012, 2012.

Schmid, H.P.: Source areas for scalars and scalar fluxes. Boundary-Layer Meteorol., **67,** 293–318, https://doi.org/10.1007/BF00713146, 1994.

Shephard, M. W., McLinden, C. A., Cady-Pereira, K. E., Luo, M., Moussa, S. G., Leithead, A., Liggio, J., Staebler, R. M., Akingunola, A., Makar, P., Lehr, P., Zhang, J., Henze, D. K., Millet, D. B., Bash, J. O., Zhu, L., Wells, K. C., Capps, S. L., Chaliyakunnel, S., Gordon, M., Hayden, K., Brook, J. R., Wolde, M., and Li, S. M.: Tropospheric Emission Spectrometer (TES) satellite observations of ammonia, methanol, formic acid, and carbon monoxide over the Canadian oil sands: Validation and model evaluation, Atmos. Meas. Tech., 8, 5189-5211, https://doi.org/10.5194/amt-8-5189-2015, 2015.

Shonkwiler, K. B., and Ham, J. M.: Ammonia emissions from a beef feedlot: Comparison of inverse modeling techniques using long-path and point measurements of fenceline NH_3, Agric. For. Meterol., 258, 29-42, https://doi.org/10.1016/j.agrformet.2017.10.031, 2018.

Siddique, T., Fedorak, P. M., MacKinnon, M. D., and Foght, J. M.: Metabolism of BTEX and Naphtha Compounds to Methane in Oil Sands Tailings, Environmental Science & Technology, 41, 2350-2356, 10.1021/es062852q, 2007.

Siddique, T., Penner, T., Semple, K., and Foght, J. M.: Anaerobic biodegradation of longer-chain n-alkanes coupled to methane production in oil sands tailings, Environ. Sci. Tech., 45, 5892-5899, https://doi.org/10.1021/es200649t, 2011.

Siddique, T., Penner, T., Klassen, J., Nesbø, C., and Foght, J. M.: Microbial communities involved in methane production from hydrocarbons in oil sands tailings, Environ. Sci. Tech., 46, 9802-9810, https://doi.org/10.1021/es302202c, 2012.

Simpson, I. J., Blake, N. J., Barletta, B., Diskin, G. S., Fuelberg, H. E., Gorham, K., Huey, L. G., Meinardi, S., Rowland, F. S., Vay, S. A., Weinheimer, A. J., Yang, M., and Blake, D. R.: Characterization of trace gases measured over Alberta oil sands mining operations: 76 speciated C_2–C_{10} volatile organic compounds (VOCs), CO_2, CH_4, CO, NO, NO_2, NO_y, O_3 and SO_2, Atmos. Chem. Phys., 10, 11931-11954, https://doi.org/10.5194/acp-10-11931-2010, 2010.

Simpson, I. J., Akagi, S. K., Barletta, B., Blake, N. J., Choi, Y., Diskin, G. S., Fried, A., Fuelberg, H. E., Meinardi, S., Rowland, F. S., Vay, S. A., Weinheimer, A. J., Wennberg, P. O., Wiebring, P., Wisthaler, A., Yang, M., Yokelson, R. J., and Blake, D. R.: Boreal forest fire emissions in fresh Canadian smoke plumes: C_1-C_{10} volatile organic compounds (VOCs), CO_2, CO, NO_2, NO, HCN and CH_3CN, Atmos. Chem. Phys., 11, https://doi.org/6445-6463, 10.5194/acp-11-6445-2011, 2011.

Small, C. C., Cho, S., Hashisho, Z., and Ulrich, A. C.: Emissions from oil sands tailings ponds: Review of tailings pond parameters and emission estimates, Journal of Petroleum Science and Engineering, 127, 490-501, https://doi.org/10.1016/j.petrol.2014.11.020, 2015.

Smith, T. E. L., Paton-Walsh, C., Meyer, C. P., Cook, G. D., Maier, S. W., Russell-Smith, J., Wooster, M. J., and Yates, C. P.: New emission factors for Australian vegetation fires measured using open-path Fourier Transform

Infrared spectroscopy - Part 2: Australian tropical savanna fires, Atmos. Chem. Phys., 14, https://doi.org/11335-11352, 10.5194/acp-14-11335-2014, 2014.

Thoma, E. D., Green, R. B., Hater, G. R., Goldsmith, C. D., Swan, N. D., Chase, M. J., and Hashmonay, R. A.: Development of EPA OTM 10 for landfill applications, J. Environ. Eng., 136, 769-776, https://doi.org/10.1061/(ASCE)EE.1943-7870.0000157, 2010.

Whaley, C. H., Makar, P. A., Shephard, M. W., Zhang, L., Zhang, J., Zheng, Q., Akingunola, A., Wentworth, G. R., Murphy, J. G., Kharol, S. K., and Cady-Pereira, K. E.: Contributions of natural and anthropogenic sources to ambient ammonia in the Athabasca Oil Sands and north-western Canada, Atmos. Chem. Phys., 18, 2011-2034, https://doi.org/10.5194/acp-18-2011-2018, 2018.

Wiacek, A., Li, L., Tobin, K., and Mitchell, M.: Characterization of trace gas emissions at an intermediate port, Atmos. Chem. Phys., 18, 13787-13812, https://doi.org/10.5194/acp-18-13787-2018, 2018.

Wu, R. T., Chang, S.-Y., Chung, Y. W., Tzou, H. C., and Tso, T.-L.: FTIR remote sensor measurements of air pollutants in the petrochemical industrial park, Proc. SPIE 2552, Infrared Technology XXI, 1995, 719-727, https://doi.org/10.1117/12.218271, 1995.

Yeh, S., Jordaan, S. M., Brandt, A. R., Turetsky, M. R., Spatari, S., and Keith, D. W.: Land use greenhouse gas emissions from conventional oil production and oil sands, Environ. Sci. Tech., 44, 8766-8772, https://doi.org/10.1021/es1013278, 2010.

Yokelson, R. J., Griffith, D. W. T., and Ward, D. E.: Open-path Fourier Transform Infrared studies of large-scale laboratory biomass fires, J. Geophys. Res. Atmos., 101, 21067-21080, https://doi.org/10.1029/96JD01800, 1996.

Yokelson, R. J., Susott, R., Ward, D. E., Reardon, J., and Griffith, D. W. T.: Emissions from smoldering combustion of biomass measured by open-path Fourier Transform Infrared spectroscopy, J. Geophys. Res. Atmos., 102, 18865-18877, https://doi.org/10.1029/97JD00852, 1997.

Yokelson, R. J.: Emissions of formaldehyde, acetic acid, methanol, and other trace gases from biomass fires in North Carolina measured by airborne Fourier Transform Infrared spectroscopy, J. Geophys. Res. Atmos., 104, 30109-30125, https://doi.org/10.1029/1999JD900817, 1999.

Yokelson, R. J., Karl, T., Artaxo, P., Blake, D. R., Christian, T. J., Griffith, D. W. T., Guenther, A., and Hao, W. M.: The tropical forest and fire emissions experiment: Overview and airborne fire emission factor measurements, Atmos. Chem. Phys., 7, 5175-5196, https://doi.org/10.5194/acp-7-5175-2007, 2007.

Yokelson, R. J., Burling, I. R., Gilman, J. B., Warneke, C., Stockwell, C. E., De Gouw, J., Akagi, S. K., Urbanski, S. P., Veres, P., Roberts, J. M., Kuster, W. C., Reardon, J., Griffith, D. W. T., Johnson, T. J., Hosseini, S., Miller, J. W., Cocker Iii, D. R., Jung, H., and Weise, D. R.: Coupling field and laboratory measurements to estimate the emission factors of identified and unidentified trace gases for prescribed fires, Atmos. Chem. Phys., 13, 89-116, https://doi.org/10.5194/acp-13-89-2013, 2013.

You, Y., Staebler, R. M., Moussa, S. G., Su, Y., Munoz, T., Stroud, C., Zhang, J., and Moran, M. D.: Long-path measurements of pollutants and micrometeorology over Highway 401 in Toronto, Atmos. Chem. Phys., 17, 14119-14143, https://doi.org/10.5194/acp-17-14119-2017, 2017.

https://doi.org/10.5194/amt-2020-257
Preprint. Discussion started: 6 August 2020

You, Y., Staebler, R. M.: Moussa, S. G., Beck, J., Mittermeier, R. L.: Methane emissions from an oil sands tailings pond: A quantitative comparison of fluxes derived by different methods, Atmos. Meas. Tech. Discuss., https://doi.org/10.5194/amt-2020-116, in review, 2020.

605 Zhang, L., Cho, S., Hashisho, Z., and Brown, C.: Quantification of fugitive emissions from an oil sands tailings pond by eddy covariance, Fuel, 237, 457-464, https://doi.org/10.1016/j.fuel.2018.09.104, 2019.

https://doi.org/10.5194/amt-2020-257
Preprint. Discussion started: 6 August 2020

Atmospheric Measurement Techniques Discussions

Tables

Table 1 Spectral windows of OP- FTIR spectra for retrieving mole fractions of pollutants in this study.

Pollutant name	Chemical formula	Spectral Window (cm^{-1})	Interference gases	Threshold correlation coefficient[a]	Detection limit[c]	Paths
Methane	CH_4	3006-3021	H_2O	0.95	1.1 ppb	All three
Ammonia	NH_3	957-973	H_2O, CO_2	0.3	1.1 ppb	All three
Methanol	CH_3OH	1020-1040	H_2O, NH_3, O_3, C_2H_5OH, C_6H_6	0.3	1.1 ppb	All three
Butane[b]	n-C_4H_{10}	2804-3001	H_2O, CH_4, CH_3OH, HCHO, n-C_7H_{16}, n-C_6H_{14}, n-C_8H_{18}, $CH_3CH(CH_3)C_3H_7$	0.1	1.1 ppb	All three
Octane[b]	n-C_8H_{18}	2804-3001	H_2O, CH_4, CH_3OH, HCHO, n-C_7H_{16}, n-C_6H_{14}, $CH_3CH(CH_3)C_3H_7$, $C_2H_5CH(CH_3)C_2H_5$	0.1	0.9 ppb	All three
Formaldehyde	HCHO	2730-2800	H_2O, CO_2, CH_4	0.2	2.3 ppb	Bottom only
Carbon dioxide	CO_2	2030-2133	H_2O, CO	0.8	-	Bottom only

[a] Threshold correlation coefficient is a input for OPUS_RS when performing fitting analysis of FTIR spectra. When the correlation coefficient between measured spectrum and reference spectrum with the defined spectral window is below this threshold, that pollutant is not "identified" and the mole fraction is reported as zero in OPUS_RS (You et al., 2017).

[b] Butane and octane mixing ratio are quantified as two surrogates to quantify a "total alkane" mixing ratio = Butane + Octane (Thoma et al., 2010).

[c] Detection limit is calculated by converting 3σ of the noise of the measurements with a retroreflector distance of 225m by Bruker to 3σ of the noise with 200m in this study.

https://doi.org/10.5194/amt-2020-257
Preprint. Discussion started: 6 August 2020

Atmospheric Measurement Techniques Discussions

620 Table 2 Summary of fluxes from OP-FTIR measurements. Results are area weight-averaged fluxes from the pond.

All fluxes in g $m^{-2}d^{-1}$	Flux method	Q_25%	Median	Q_75%	Mean[a]
CH_4	Tower EC	4.2	5.9	7.9	6.1± 0.5
	FTIR gradient	1.9	3.4	5.5	3.7 ± 0.5
	IDM	3.6	5.2	6.6	5.4± 0.4
NH_3	gradient	0.01	0.04	0.08	0.05 ± 0.01
	IDM	0.06	0.09	0.15	0.11 ± 0.01
Total alkane	gradient	0.25	0.95	1.97	1.33 ± 0.19
	IDM	0.57	0.94	1.56	1.33 ± 0.10

[a] Errors with the mean fluxes are calculated with a "top-down" approach: the average of standard deviations of fluxes from five periods when the fluxes were relatively steady.

https://doi.org/10.5194/amt-2020-257
Preprint. Discussion started: 6 August 2020

Atmospheric Measurement Techniques Discussions

625 **Figures**

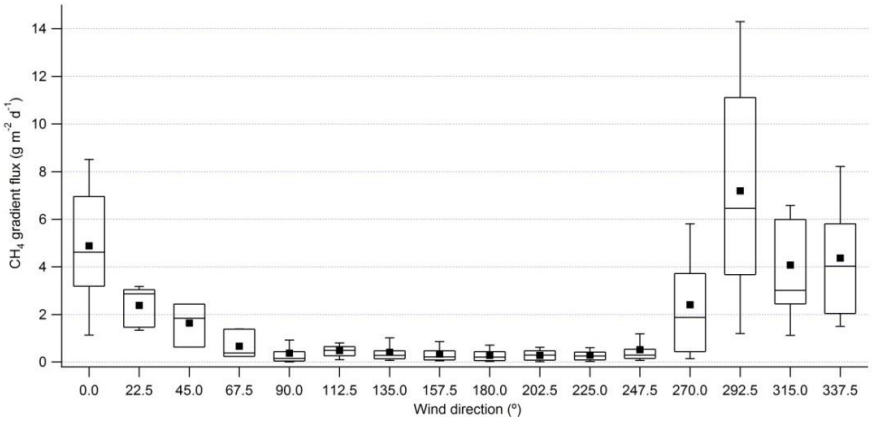

Figure 1 Gradient flux of CH_4 from FTIR binned by wind direction in 22.5-degree bins

https://doi.org/10.5194/amt-2020-257
Preprint. Discussion started: 6 August 2020

Atmospheric Measurement Techniques Discussions

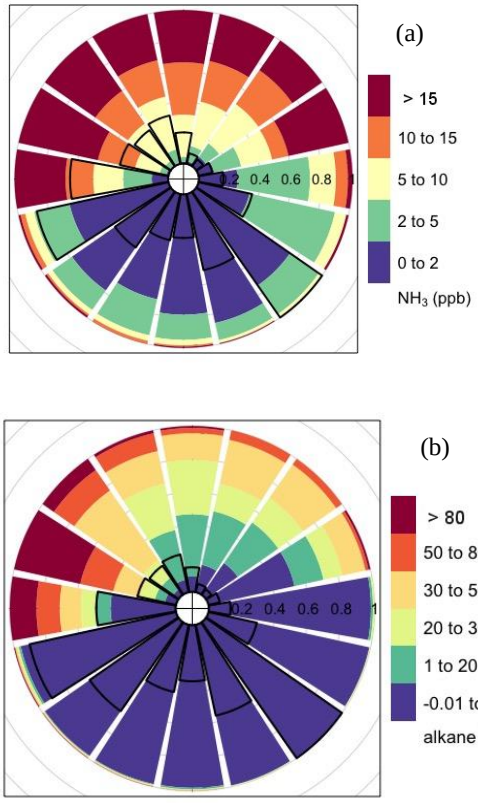

630

Figure 2 Normalised rose plot of NH_3 (a) and total alkane (b) mole fractions from FTIR bottom path. Colors represent mole fraction in ppb. The length of each colored segment presents the time fractions of that mole fraction range in each direction bin. The radius of the black open sectors indicates the frequency of wind in each direction bin; angle represents wind direction.

635

https://doi.org/10.5194/amt-2020-257
Preprint. Discussion started: 6 August 2020

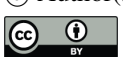

Atmospheric Measurement Techniques Discussions

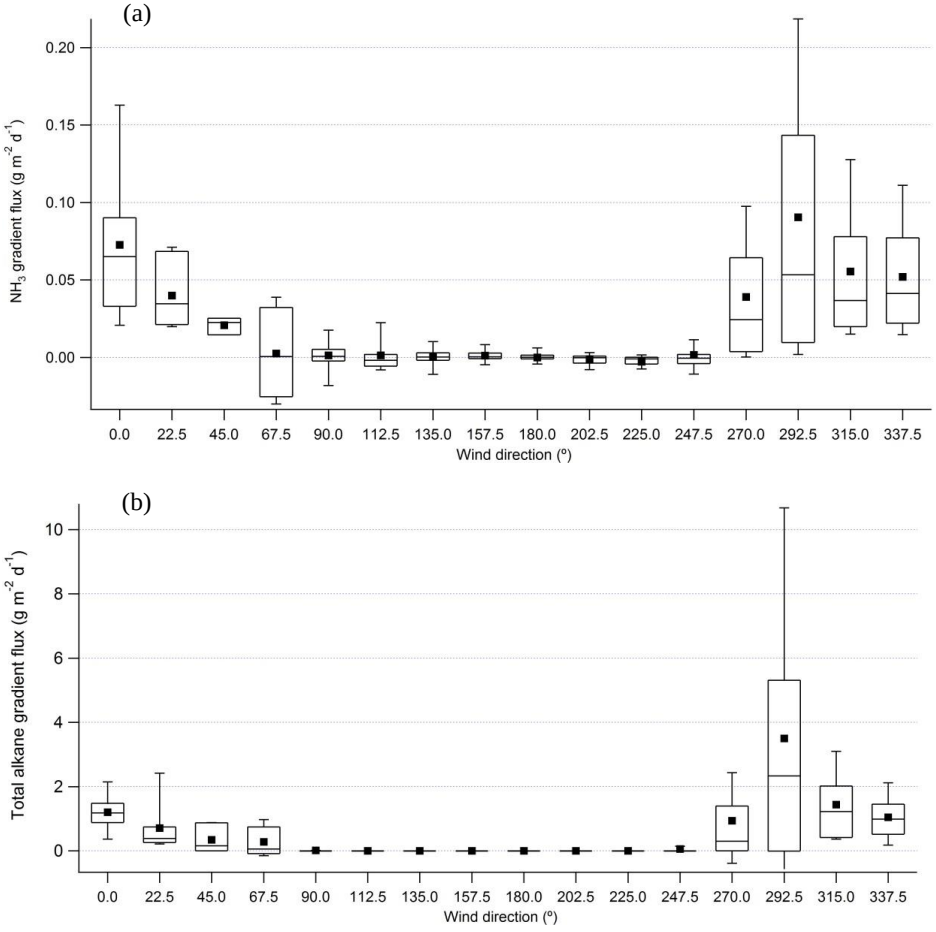

640 **Figure 3 Gradient flux of NH_3 (a) and total alkane (b) from FTIR top-bottom path binned by wind direction in 22.5-degree bins.**

https://doi.org/10.5194/amt-2020-257
Preprint. Discussion started: 6 August 2020

Atmospheric Measurement Techniques Discussions

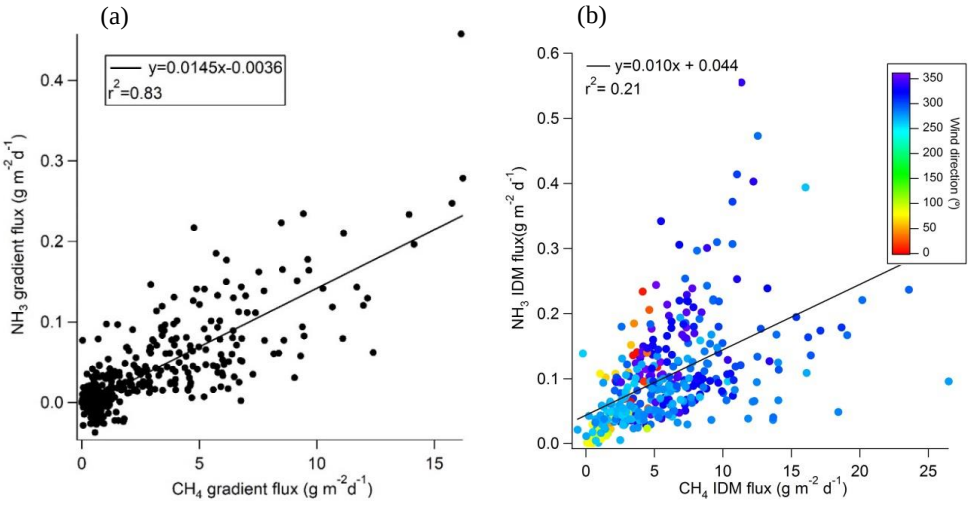

Figure 4 (a): NH_3 gradient flux compared to CH_4 gradient flux; (b): NH_3 IDM flux compared to CH_4 IDM flux